Cell

Role of PFKFB3-Driven Glycolysis in Vessel Sprouting

Katrien De Bock,[1,10,20] Maria Georgiadou,[1,10,20] Sandra Schoors,[1,10] Anna Kuchnio,[1,10] Brian W. Wong,[1,10] Anna Rita Cantelmo,[1,10] Annelies Quaegebeur,[1,10] Bart Ghesquière,[1,10] Sandra Cauwenberghs,[1,10] Guy Eelen,[1,10] Li-Kun Phng,[2,11] Inge Betz,[1,10] Bieke Tembuyser,[1,10] Katleen Brepoels,[1,10] Jonathan Welti,[1,10] Ilse Geudens,[2,11] Inmaculada Segura,[1,10] Bert Cruys,[1,10] Franscesco Bifari,[1,10] Ilaria Decimo,[1,10] Raquel Blanco,[14] Sabine Wyns,[1,10] Jeroen Vangindertael,[3] Susana Rocha,[3] Russel T. Collins,[14] Sebastian Munck,[4,12] Dirk Daelemans,[5] Hiromi Imamura,[15] Roland Devlieger,[6] Mark Rider,[16] Paul P. Van Veldhoven,[7] Frans Schuit,[8] Ramon Bartrons,[17] Johan Hofkens,[3] Peter Fraisl,[1,9,10,13] Sucheta Telang,[18] Ralph J. DeBerardinis,[19] Luc Schoonjans,[1,10] Stefan Vinckier,[1,10] Jason Chesney,[18] Holger Gerhardt,[2,11,14] Mieke Dewerchin,[1,10] and Peter Carmeliet[1,10,*]

[1]Laboratory of Angiogenesis and Neurovascular Link, Vesalius Research Center, Department of Oncology
[2]Vascular Patterning Laboratory, Vesalius Research Center, Department of Oncology
[3]Molecular Imaging and Photonics Laboratory
[4]Center for Human Genetics
[5]Laboratory of Virology and Chemotherapy, Rega Institute
[6]Department of Gynaecology and Obstetrics
[7]Laboratory of Lipid Biochemistry and Protein Interactions
[8]Gene Expression Unit
[9]Laboratory of Cell Proliferation, Vesalius Research Center, Department of Oncology
University of Leuven, Leuven 3000, Belgium
[10]Laboratory of Angiogenesis and Neurovascular Link, Vesalius Research Center
[11]Vascular Patterning Laboratory, Vesalius Research Center
[12]Center for the Biology of Disease
[13]Laboratory of Cell Proliferation, Vesalius Research Center
VIB, Leuven 3000, Belgium
[14]Vascular Biology Laboratory, London Research Institute, Cancer Research UK, London WC2A 3LY, UK
[15]The Hakubi Center for Advanced Research and Graduate School of Biostudies, Kyoto University, Kyoto 606-8501, Japan
[16]Hormone and Protein Phosphorylation Research Laboratory, De Duve Institute, Université de Louvain, Brussels 1200, Belgium
[17]Departament de Ciències Fisiològiques II, Universitat de Barcelona, IDIBELL, Barcelona 08907, Spain
[18]James Graham Brown Cancer Center, University of Louisville, Louisville, KY 40202, USA
[19]Children's Medical Center Research Institute, University of Texas Southwestern Medical Center, Dallas, TX 75390-8502, USA
[20]These authors contributed equally to this work
*Correspondence: peter.carmeliet@vib-kuleuven.be
http://dx.doi.org/10.1016/j.cell.2013.06.037

SUMMARY

Vessel sprouting by migrating tip and proliferating stalk endothelial cells (ECs) is controlled by genetic signals (such as Notch), but it is unknown whether metabolism also regulates this process. Here, we show that ECs relied on glycolysis rather than on oxidative phosphorylation for ATP production and that loss of the glycolytic activator PFKFB3 in ECs impaired vessel formation. Mechanistically, PFKFB3 not only regulated EC proliferation but also controlled the formation of filopodia/lamellipodia and directional migration, in part by compartmentalizing with F-actin in motile protrusions. Mosaic in vitro and in vivo sprouting assays further revealed that PFKFB3 overexpression overruled the pro-stalk activity of Notch, whereas PFKFB3 deficiency impaired tip cell formation upon Notch blockade, implying that glycolysis regulates vessel branching.

INTRODUCTION

Vessel sprouting relies on the induction of endothelial cells (ECs) into specialized subtypes, each performing specific functions. Tip cells at the forefront of the vascular branch extend long filopodia and navigate but rarely proliferate, whereas trailing stalk cells proliferate to elongate the branch (Geudens and Gerhardt, 2011; Potente et al., 2011). Once the vessel is perfused, ECs become quiescent phalanx cells. Several genetic factors coordinate tip, stalk, and phalanx cell phenotypes (Geudens and Gerhardt, 2011; Potente et al., 2011). For instance, Notch signaling potently controls vessel branching by stimulating the stalk cell phenotype (Potente et al., 2011). Hence, blockade of Notch signaling induces vascular hypersprouting, while activation of the Notch pathway causes the opposite effect. However, a role for metabolism in vessel sprouting has not been studied to date.

Only a limited number of reports have characterized the metabolic pathways in ECs in vitro, and even fewer reports have studied how EC metabolism regulates angiogenesis in vivo (Dobrina and Rossi, 1983; Harjes et al., 2012; Laing et al., 1992; Mertens et al., 1990; Peters et al., 2009). Despite immediate access to oxygen in the blood, ECs have been reported to rely on glycolysis (Dobrina and Rossi, 1983; Krützfeldt et al., 1990; Mertens et al., 1990). However, other studies have claimed that glutamine and fatty acids were more essential substrates, suggesting an important role for oxidative phosphorylation and mitochondrial respiration (Leighton et al., 1987; Spolarics et al., 1991). How critical glycolysis versus respiration is for EC behavior in vivo is unknown.

One of the rate-limiting checkpoints of the glycolytic flux is the conversion of fructose-6-phosphate (F6P) to fructose-1,6-bisphosphate (F1,6P_2) by 6-phosphofructo-1-kinase (PFK-1). Phosphofructokinase-2/fructose-2,6-bisphosphatase (PFKFB) enzymes synthesize fructose-2,6-bisphosphate (F2,6P_2), an allosteric activator of PFK-1 and the most potent stimulator of glycolysis (Van Schaftingen et al., 1982). Of all PFKFB isoenzymes, PFKFB3 has a much higher kinase activity than bisphosphatase activity (700-fold), thus favoring the production of intracellular F2,6P_2 levels and controlling its abundance (Yalcin et al., 2009b). By contrast, the PFKFB4 isoenzyme has a much weaker kinase activity and has been reported to stimulate or inhibit glycolysis (Goidts et al., 2012; Ros et al., 2012). Silencing as well as pharmacological inhibition of PFKFB3 in tumor cells reduces tumor cell glycolysis and growth (Chesney et al., 1999; Clem et al., 2008). However, aside from a single study documenting its expression in ECs (Bando et al., 2005), the role of PFKFB3 in angiogenesis has not been studied. Here, we investigated whether PFKFB3-driven glycolysis regulates vessel sprouting and whether it affects tip versus stalk cell formation.

RESULTS

Endothelial Cells Are Highly Glycolytic

We first explored which metabolic pathway is critical for ECs and measured the flux of metabolic pathways using radioactive tracer-labeled substrates in EC monolayers. Arterial, venous, lymphatic, and microvascular ECs were highly glycolytic (Figure 1A). Glycolysis was even higher in hemangioma and angiosarcoma cells (Figure 1B). Glycolysis levels in ECs were largely comparable to those in tumor cells but much higher than in various other healthy cells (Figures 1A and 1B). For most experiments, human umbilical venous endothelial cells (HUVECs) were used (further denoted as "ECs"). Notably, when compared to glucose oxidation (GO), fatty acid oxidation (FAO), and glutamine oxidation (QO), glycolytic flux was >200-fold higher (Figure 1C). Mitochondrial respiration was lower in ECs than in other oxidative cell types (Figure 1D). Calculation of the amount of ATP showed that glycolysis generated up to 85% of the total cellular ATP content. Overall, glycolysis is the predominant bioenergetic pathway for ECs.

PFKFB3 Regulates Glycolysis in ECs

To explore the functional importance of glycolysis in ECs, we focused on PFKFB3, the most abundant isoenzyme in various EC subtypes (Figures S1A–S1D available online). PFKFB3 silencing in EC monolayers with a lentiviral vector encoding a PFKFB3 small hairpin RNA (shRNA) (PFKFB3^{KD}) lowered PFKFB3 protein levels by 76% (Figure S1E). PFKFB3 knockdown decreased F2,6P_2 levels (Figure S1F); it also reduced glycolytic flux but by no more than 35% (Figure 1E). Similar effects were obtained when using PFKFB3-selective RNA interference (RNAi) oligomers, which lowered PFKFB3 protein levels by 84% (Figure S1G) and reduced glycolysis by 40% (Figure 1E). PFKFB3 silencing also reduced glycolysis in arterial and microvascular ECs, as well as in hemangioma and angiosarcoma cells (Figure 1E). Furthermore, PFKFB3 knockdown decreased F2,6P_2 levels in arterial ECs (by 60%) and in hemangioma cells (by 66%).

PFKFB3 Stimulates Vessel Sprouting In Vitro

To study the role of PFKFB3 in vessel formation in vitro, we first used EC spheroids. PFKFB3^{KD} decreased sprout numbers and shortened sprout length (Figures 1F–1I). Conversely, overexpression of PFKFB3 using a lentiviral vector encoding PFKFB3 (PFKFB3^{OE}) enhanced glycolysis and increased sprout numbers and length (Figures S1H–S1L). The reduced sprouting of PFKFB3-silenced ECs was partly due to an impairment of EC proliferation (Figure 1J) (see below for effects on EC motility).

In contrast, poisoning mitochondrial respiration by using inhibitors at concentrations that lower oxygen consumption did not inhibit vessel sprouting (Figures 1K and 1L; Figure S1M). Conversely, supplements of pyruvate or NADH at concentrations that increased the oxygen consumption rate failed to affect vessel sprouting and did not rescue sprouting upon PFKFB3 silencing (Figures 1M and 1N; Figure S1N). Thus, loss- and gain-of-function studies highlighted that glycolysis, rather than respiration, regulates vessel sprouting.

PFKFB3 Gene Deletion in ECs Causes Vascular Defects In Vivo

We then studied the effects of PFKFB3 deficiency on vessel formation in the postnatal mouse retina. We generated PFKFB3$^{lox/lox}$ mice and crossed them with VE-cadherin(PAC)-Cre^{ERT2} mice, an EC-specific Cre-driver line (Benedito et al., 2009), termed PFKFB3$^{v\Delta EC}$ mice. To evaluate the recombination efficiency, we crossed PFKFB3$^{v\Delta EC}$ mice with mT/mG mice, a double-fluorescent Cre reporter line that expresses membrane-targeted Tomato (mT) prior to Cre-mediated excision and GFP (mG) after excision. Treatment of triple-transgenic pups with tamoxifen at postnatal days 1–4 inactivated PFKFB3 in 50%–85% of ECs, and the PFKFB3-lox allele was correctly recombined (Figure S2A). EC loss of PFKFB3 diminished the number of branch points, distal sprouts with filopodia and filopodia (Figures 2A–2H). Distal sprouts in PFKFB3$^{v\Delta EC}$ mice also had fewer side connections. The radial expansion of the vascular plexus was reduced in PFKFB3$^{v\Delta EC}$ mice (Figure 2I) to similar levels as in other models with sprouting defects (Graupera et al., 2008; Phng et al., 2009). Similar results were obtained when using Pdgfb-Cre^{ERT2} mice, another EC-selective inducible Cre-driver line (Claxton et al., 2008) (Figures S2A–S2G), termed PFKFB3$^{p\Delta EC}$ mice. In PFKFB3$^{\Delta EC}$ mice, vessel regression was increased because collagen IV staining showed that there were more empty sleeves of basement membrane without ECs (Figures 2J–2L), whereas EC proliferation was reduced, as revealed

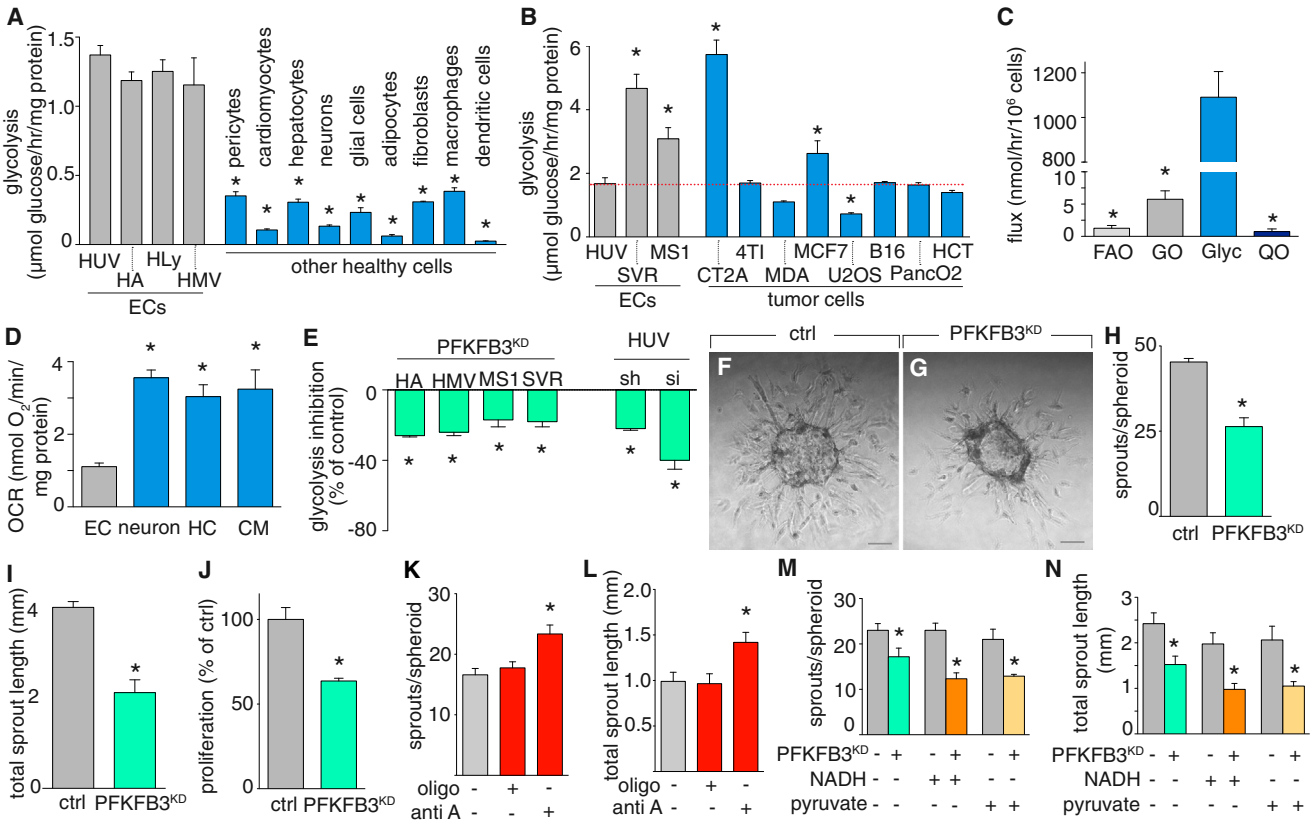

Figure 1. PFKFB3 Regulates Glycolysis and Vessel Sprouting In Vitro

(A) Glycolytic flux in venous (HUV), arterial (HA), lymphatic (HLy), or microvascular (HMV) ECs is higher than in other healthy cells (mean ± SEM; n = 3–5; *p < 0.05 versus HUV).

(B) Glycolysis in primary ECs (HUVEC) is lower than in murine angiosarcoma (SVR) and hemangioma (MS1) cells but comparable to various tumor cell lines (CT2A mouse glioma, 4T1 mouse breast carcinoma, MDA-MB-231 human breast carcinoma, MCF7 human breast adenocarcinoma, U2OS human osteosarcoma, B16F10.9 mouse melanoma, PancO2 mouse pancreatic carcinoma, and HCT116 human colon carcinoma) (mean ± SEM; n = 3; *p < 0.05 versus HUV).

(C) Flux analysis of ECs showing that glycolysis (Glyc) is higher than glucose oxidation (GO), fatty acid oxidation (FAO), or glutamine oxidation (QO) (mean ± SEM; n = 3; *p < 0.001 versus Glyc).

(D) Oxygen consumption rate (OCR) showing lower respiration in ECs than in oxidative cell types (neurons, hepatocytes [HC], and cardiomyocytes [CM]) (mean ± SEM; n = 11; *p < 0.01).

(E) Reduction in glycolysis in human arterial (HA), human microvascular (HMV), murine hemangioma (MS1), murine angiosarcoma (SVR), and human venous (HUVECs) ECs upon genetic silencing by using shRNA (PFKFB3^{KD}; sh) or small interfering RNA (si) (mean ± SEM; n = 3; *p < 0.05 versus shCtrl or siCtrl).

(F and G) Representative bright field photographs of EC spheroids showing that PFKFB3-silenced (PFKFB3^{KD}) ECs formed fewer and shorter sprouts. Scale bars, 50 μm.

(H and I) Morphometric analysis revealing that PFKFB3 silencing (PFKFB3^{KD}) reduced the number of sprouts per spheroid (H), as well as total sprout length (I) (mean ± SEM; n = 30; *p < 0.01).

(J) ^{3}H-thymidine incorporation assay showing that PFKFB3 silencing (PFKFB3^{KD}) reduced proliferation of EC monolayers (mean ± SEM, n = 3, *p < 0.01).

(K and L) Morphometric quantification revealing that inhibition of mitochondrial respiration by oligomycin (oligo) or antimycin A (anti A) did not inhibit spheroid sprouting (mean ± SEM; n = 30; *p < 0.05 versus untreated spheroids).

(M and N) Morphometric quantification revealing that stimulation of oxygen consumption by supplementation of pyruvate or NADH did not affect spheroid sprouting or rescue the reduced sprouting upon PFKFB3 blockade (mean ± SEM; n = 30; *p < 0.05 in PFKFB3^{KD} cells versus control cells).

See also Figure S1.

by the injection of EdU (Figures 2M–2O). However, EC depletion of PFKFB3 did not alter the coverage by NG2^{+} pericytes (Figures S2H–S2J).

We also analyzed the role of PFKFB3 in vessel formation in the hindbrain, another model used to study angiogenesis (Fantin et al., 2013). To assess whether PFKFB3 deficiency affected this process, we generated high (>90%) chimeric mice by injecting mCherryRed^{+} wild-type (WT) or PFKFB3$^{-/-}$ ES cells in CD-1 blastocysts. The vascular area in the ventricular zone was reduced by 40% in embryonic day 10.5 (E10.5) somite-matched PFKFB3$^{-/-}$ chimeras (Figures 2P–2R), indicating that PFKFB3 regulated vessel sprouting.

PFKFB3 Silencing Impairs Lamellipodia Formation

We then explored whether the vascular defects in mice lacking endothelial PFKFB3 were also due to EC motility defects, aside

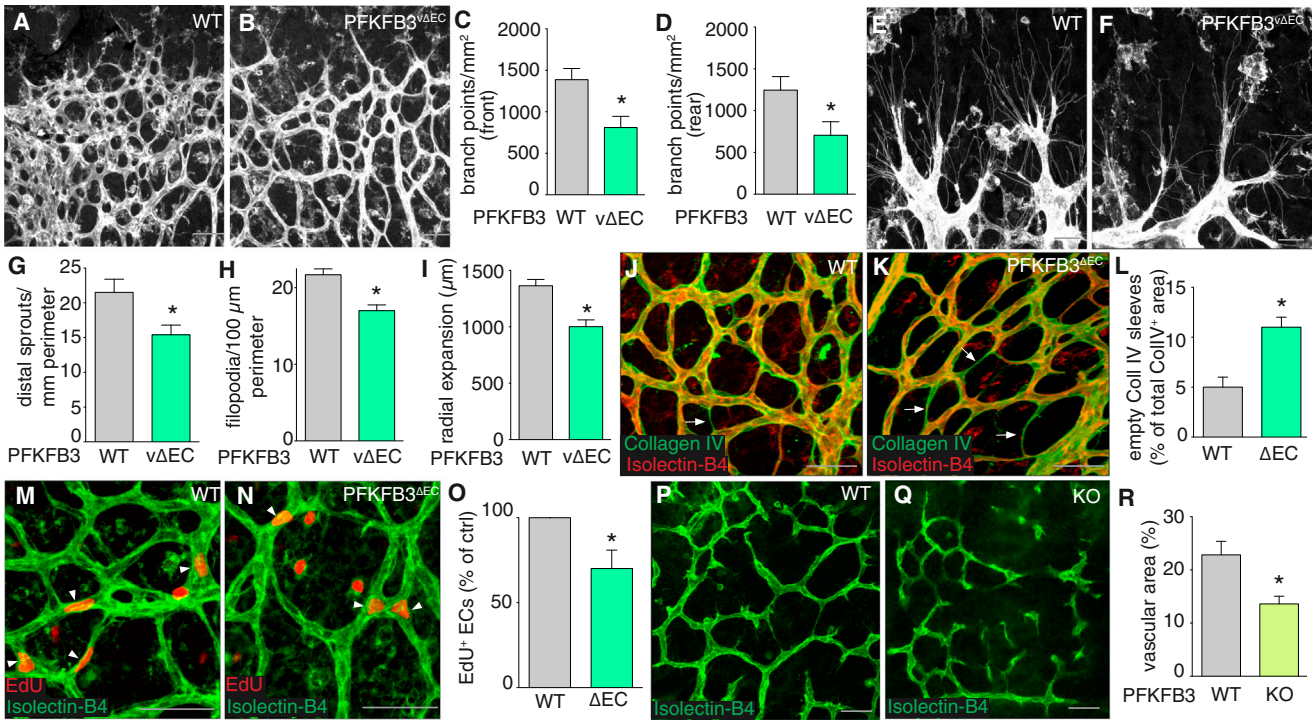

Figure 2. PFKFB3 Gene Deletion in ECs Causes Vascular Defects In Vivo

(A and B) Confocal images of isolectin-B4-stained (gray) retinal vessels of postnatal day 5 (P5) pups showing reduced vascular branching in mice with endothelial PFKFB3 deficiency (PFKFB3$^{v\Delta EC}$) (B) as compared to wild-type (WT) mice (A). Scale bars, 50 μm.

(C and D) Quantification of the number of branch points at the front (C) or rear (D) in the retinal vasculature of PFKFB3$^{v\Delta EC}$ mice (mean ± SEM; n = 20; *p < 0.03).

(E and F) High-magnification confocal images of retinal vessels at the vascular front in WT (E) or PFKFB3$^{v\Delta EC}$ (F) pups showing fewer filopodia in PFKFB3$^{v\Delta EC}$ pups. Scale bars, 20 μm.

(G and H) Quantification of distal sprouts with filopodia (G) and the number of filopodia (H) in the retinal vasculature of PFKFB3$^{v\Delta EC}$ mice (mean ± SEM; n = 7–9; *p < 0.05).

(I) Quantification of retinal vascular outgrowth showing that endothelial PFKFB3 gene deficiency (PFKFB3$^{v\Delta EC}$) reduces radial expansion (mean ± SEM; n = 8–9; *p = 0.001).

(J–L) Isolectin-B4 (red) and collagen IV (green) staining of WT (J) and PFKFB3$^{\Delta EC}$ (K) mice showing that PFKFB3$^{\Delta EC}$ ECs had more isolectin-B4^{-} collagenIV^{+} empty sleeves (arrows). Scale bars, 50 μm. (L) The quantification of the collagenIV^{+} empty sleeves is shown (mean ± SEM; n = 5–7; *p = 0.002).

(M–O) Staining for EdU (red) and Isolectin-B4 (green), revealing fewer proliferating ECs in PFKFB3$^{\Delta EC}$ (N) than WT (M) mice. Scale bars, 50 μm. (O) The quantification of the proliferating ECs is shown (mean ± SEM; n = 9; *p < 0.05).

(P–R) Confocal images of isolectin-B4-stained (green) hindbrains showing reduced vascularization in the ventricular zone of PFKFB3$^{-/-}$ (Q) as compared to WT (P) chimeras. Scale bars, 50 μm. (R) The quantification of the vascular area is shown (mean ± SEM; n = 4; *p = 0.04).

See also Figure S2.

from the aforementioned EC proliferation defects. Because lamellipodia are critical for EC motility, we quantified lamellipodia formation. Time-lapse video imaging of GFP^{+} ECs revealed that these cells formed lamellipodial projections over large areas and had leading-edge projections with a front-to-back distribution, resulting in cell body displacement (Figures 3A, 3D, and 3G; Movie S1A). In contrast, PFKFB3-silenced cells formed smaller lamellipodia and often only formed irregularly bulging protrusions (Figures 3B, 3E, and 3G; Movie S1B). Lamellipodia in PFKFB3-silenced cells were also more transient, and the more randomly projecting disoriented protrusions were unable to produce cell displacement (Figures 3C and 3F; Movie S1B). These cells also formed fewer and shorter filopodia (Figures 3H–3M).

PFKFB3 silencing also impaired EC motility, as it reduced EC migration and sprout formation in the presence of mitomycin C (MitoC), which blocks EC proliferation (Figures 3N–3P), and decreased the EC migration velocity (Figure 3Q). Moreover, video imaging of random cell-motility tracks of individual ECs revealed a greater directional persistence of movement for control than PFKFB3-silenced cells (Figures 3R and 3S), presumably because PFKFB3-silenced ECs were unable to form sustained lamellipodia.

Tip and Stalk Cell Signals Regulate PFKFB3 Levels

We then explored how PFKFB3 regulated vessel sprouting mechanistically, and therefore first analyzed whether sprouting-governing signals affected PFKFB3 expression. Indeed, sprouting-inducing signals (VEGF, FGF2) increased PFKFB3 expression and glycolysis (Figure 4A), whereas the sprouting-limiting signal DLL4 (activating Notch) caused opposite effects (Figure 4B). However, PFKFB3 levels did not alter the genetic tip versus stalk cell signature of ECs in baseline conditions (Figures 4C and 4D).

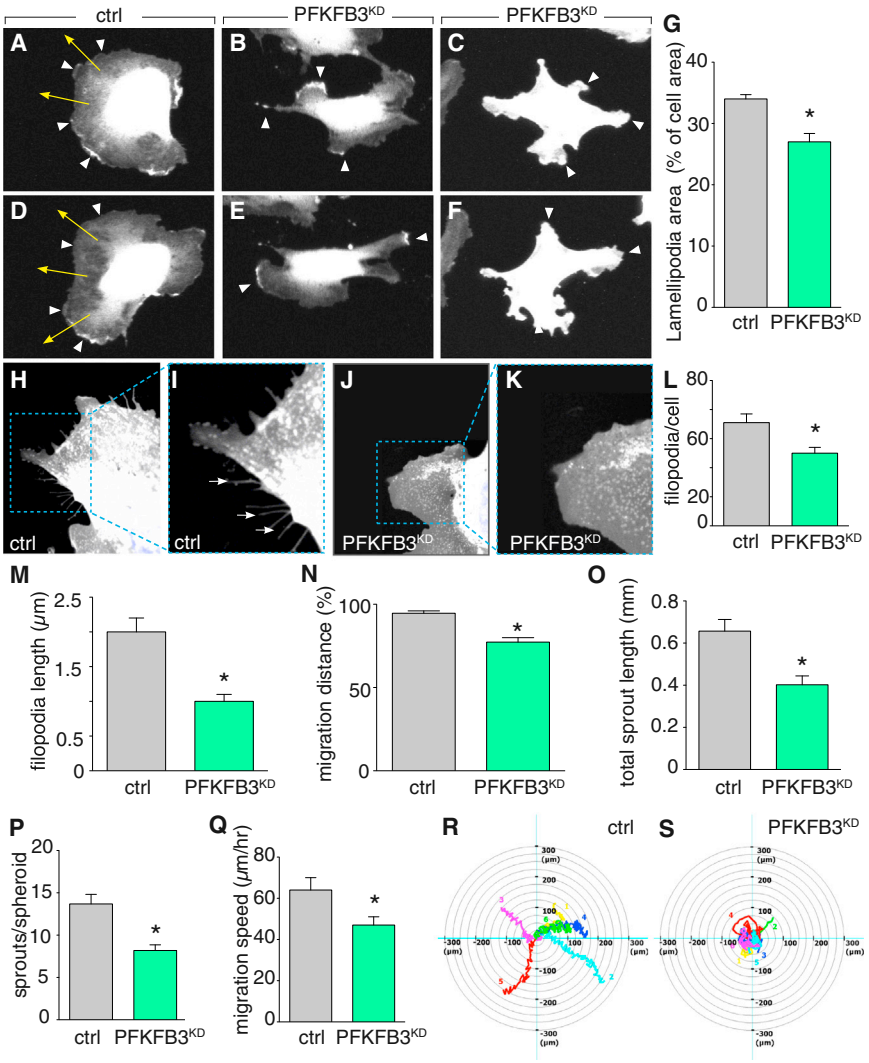

Figure 3. PFKFB3 Blockade Impairs Lamellipodia Formation

(A–G) Snapshot images of time-lapse video imaging of GFP$^+$ ECs (Movie S1) are shown to illustrate the dynamic shape and size changes of the lamellipodia and cellular protrusions in control (A and D) and PFKFB3-silenced (B, C, E, and F) cells. Arrows denote the migration direction. Lamellipodia in (A), (B), (D), and (E) are the gray veil-like structures; the nucleus and surrounding cell organelles are intense white. In control cells, note the presence of large lamellipodia uniformly forming over broad sections of the cell's perimeter (arrowheads in A and D). In PFKFB3-silenced cells, note the presence of smaller, more localized lamellipodia (arrowheads in B and E) or the irregularly bulging small protrusions (arrowheads in C and F). (G) The quantification of the lamellipodia area is shown (mean ± SEM; n = 5 independent experiments each containing >20 cells analyzed; *$p < 0.05$).

(H–M) Micrograph of ECs, stained with CellMask (gray) and nuclear DAPI (blue), showing filopodia (arrows) in control cells (H and I), but not in PFKFB3^{KD} cells (J and K). (I and K) Shown are higher magnifications of the boxes in (H) and (J), respectively. (L and M) The quantification of the number of filopodia (L) and their length (M) is shown (mean ± SEM; n = 5; *$p < 0.05$).

(N) Quantification of MitoC-treated EC migration in scratch wound assays showing reduced migration upon silencing of PFKFB3 (PFKFB3^{KD}) (mean ± SEM; n = 3; *$p < 0.05$).

(O and P) Morphometric analysis of MitoC-treated sprouting EC spheroids revealing that the effect of PFKFB3 silencing (PFKFB3^{KD}) in reducing total sprout length (O) as well as the number of sprouts per spheroid (P) is independent of proliferation (mean ± SEM; n = 30; *$p < 0.01$).

(Q) Quantification of migration speed showing reduced migration velocity upon silencing of PFKFB3 (PFKFB3^{KD}) (mean ± SEM; n = 5; *$p < 0.05$).

(R and S) Analysis of random cell-motility tracks by time-lapse imaging of GFP$^+$ ECs. Cell tracks were determined by cell nuclei position and migration origin was superimposed at the zero-cross point. Compared to the more directional persistence of cell movement in control cells (R), cell movements were more random in PFKB3-silenced (PFKFB3^{KD}) cells (S).

See also Movie S1.

Furthermore, PFKFB3 levels did not alter the molecular signature of ECs that were genetically or pharmacologically instructed to the tip or stalk cell phenotype. Indeed, we pretreated ECs with DAPT to promote a tip cell phenotype, as evidenced by the upregulation of *VEGFR2/KDR* (tip-cell-enriched gene) by 69% and downregulation of *VEGFR1* (stalk-cell-enriched signal) by 38%. However, PFKFB3 silencing did not alter the molecular signature of Notch-silenced cells (Figure 4C). Conversely, we also overexpressed the Notch intracellular domain (NICD) to promote a stalk cell phenotype, as evidenced by the upregulated Notch-target genes (Figure 4D). In stalk-promoted cells, PFKFB3 overexpression did not alter gene expression (Figure 4D).

PFKFB3 Levels Influence the Tip Cell Position

We then assessed whether PFKFB3 levels influenced the cell-autonomous ability of ECs to form tip cells. We therefore generated mosaic spheroids by mixing ECs expressing normal or silenced levels of PFKFB3 and assessed which ECs were present at the tip. PFKFB3 silencing was achieved by lentiviral transduction of shPFKFB3 and EGFP (PFKFB3$^{KD/GFP}$). These cells were mixed in a 1:1 ratio with WT cells expressing mCherry (WT^{RED}). In control spheroids, generated by mixing WT^{RED} and EGFP-positive WT cells (WT^{GFP}), comparable numbers of each genotype were identified at the tip (Figures 4E and 4G). However, when PFKFB3$^{KD/GFP}$ and WT^{RED} cells were mixed, PFKFB3$^{KD/GFP}$ cells were less frequently present at the tip (Figures 4F and 4G). Similar results were obtained when using MitoC-treated ECs, indicating that the reduced tip cell behavior of PFKFB3$^{KD/GFP}$ cells was not due to impaired proliferation (Figure S3A). Even when PFKFB3$^{KD/GFP}$ and WT^{RED} cells were mixed at a 9:1 ratio, fewer PFKFB3$^{KD/GFP}$ cells were found at the tip (Figure S3B). Conversely, elevated PFKFB3

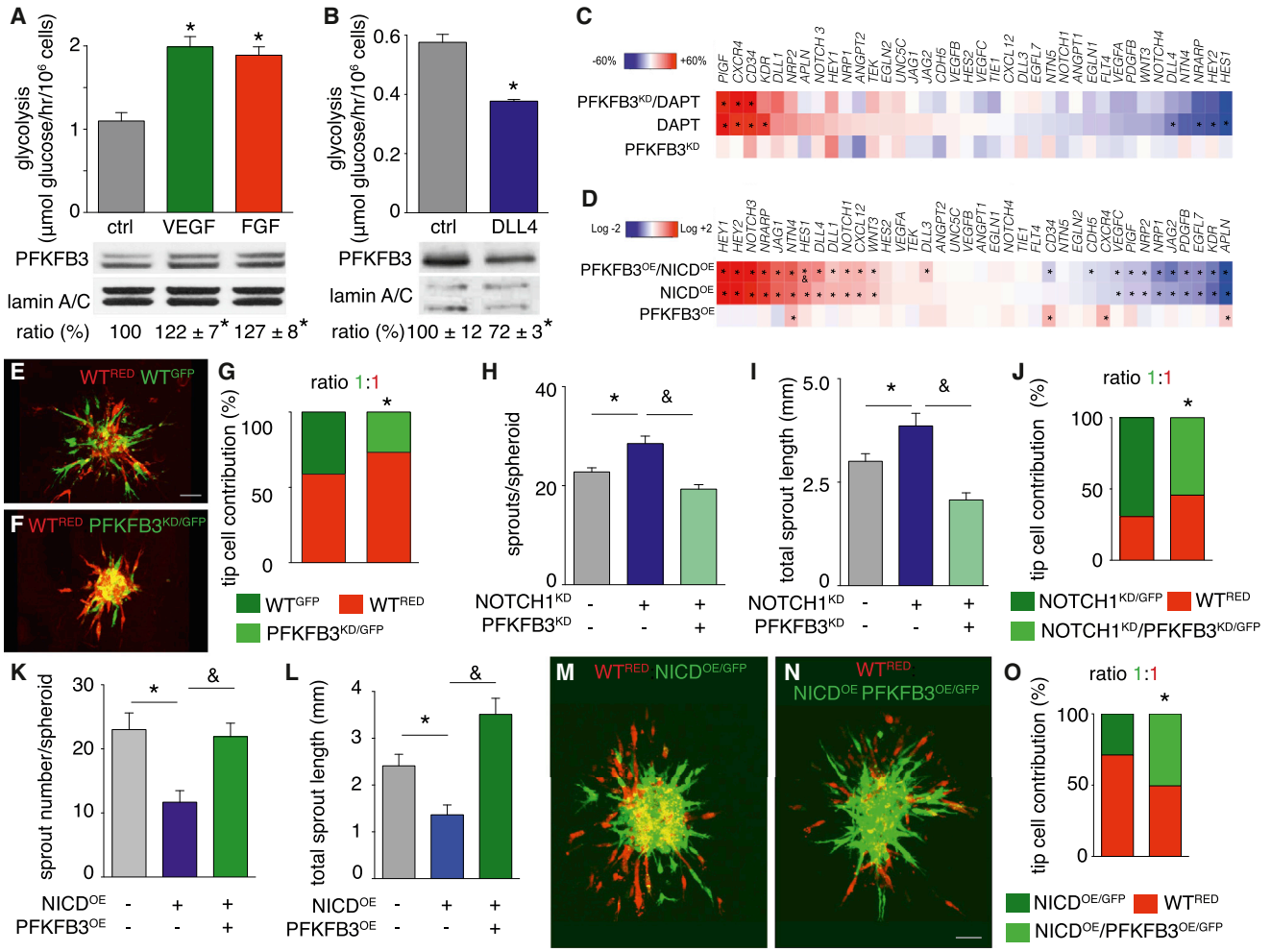

Figure 4. The Role of PFKFB3 in Tip Cell Formation

(A) Glycolytic flux analysis and western blotting showing that VEGF and FGF2 increased glycolysis (top) and PFKFB3 protein levels (bottom). Ratio represents the densitometric quantification of PFKFB3 over lamin A/C immunoreactive bands (mean ± SEM; n = 3; *p < 0.05).

(B) Glycolytic flux analysis and western blotting showing that DLL4 reduced glycolysis (top) and PFKFB3 levels (bottom). Ratio represents the densitometric quantification of PFKFB3 over lamin A/C immunoreactive bands (mean ± SEM; n = 3; *p < 0.05).

(C) Microarray analysis showing that silencing of PFKFB3 ($PFKFB3^{KD}$) in baseline conditions or after DAPT treatment did not affect the expression of sprouting-governing genes (n = 3). *p < 0.05 versus control; p was not significant for DAPT versus DAPT + $PFKFB3^{KD}$. Immunoblotting showed that VEGFR2 protein and tyrosine phosphorylation levels were not affected (data not shown).

(D) Microarray analysis showing that overexpression of PFKFB3 ($PFKFB3^{OE}$) did not affect the sprouting-governing gene signature in baseline conditions or after overexpression of the Notch intracellular domain ($NICD^{OE}$) (n = 3; *p < 0.05 versus control; &p < 0.05 versus $NICD^{OE}$).

(E–G) Representative fluorescence photographs of EC spheroids containing a 1:1 mixture of WT^{RED} and WT^{GFP} ECs showing a comparable fraction of WT^{red} and WT^{GFP} ECs at the tip position (E). In contrast, in spheroids containing a 1:1 mixture of WT^{RED} ECs and ECs with silenced PFKFB3 ($PFKFB3^{KD/GFP}$), a reduced number of $PFKFB3^{KD/GFP}$ ECs was present at the tip position (F). (G) The quantification of the fraction of tip cells with the indicated PFKFB3 genotype is shown, revealing the competitive disadvantage of $PFKFB3^{KD/GFP}$ ECs to reach the tip (n = 30; *p < 0.01). Scale bars, 50 µm.

(H and I) Morphometric quantification of spheroid sprouting showing that Notch1 silenced ($NOTCH1^{KD}$) ECs form more (H) and longer (I) sprouts but that hypersprouting was abolished when both Notch and PFKFB3 were silenced ($NOTCH1^{KD}$/$PFKFB3^{KD}$) (mean ± SEM; n = 30; *p < 0.05 versus control (gray), &p < 0.0005 versus $NOTCH1^{KD}$).

(J) Mosaic EC spheroids containing a 1:1 mixture of WT^{RED} and $NOTCH1^{KD/GFP}$ cells showing a larger fraction of $NOTCH1^{KD/GFP}$ cells at the tip (left). However, compared to WT^{RED} cells, $NOTCH1^{KD}$/ $PFKFB3^{KD/GFP}$ cells no longer have a tip cell advantage (n = 30; *p < 0.05).

(K and L) EC spheroid sprouting showing that overexpression of the Notch intracellular domain NICD ($NICD^{OE}$) reduced sprout number (K) and length (L) but that PFKFB3 ($PFKFB3^{OE}$) overcomes the impaired sprouting of $NICD^{OE}$ cells (mean ± SEM; n = 30; *p < 0.01 versus ctrl; &p < 0.01 versus $PFKFB3^{OE}$).

(M–O) Representative fluorescence photographs of mosaic EC spheroids containing a 1:1 mixture of mCherry wild-type (WT^{RED}) and GFP-labeled NICD over-expressing ($NICD^{OE/GFP}$) ECs (M) or combined NICD plus PFKFB3-overexpressing ($NICD^{OE}$/$PFKFB3^{OE/GFP}$) ECs (N), revealing that $NICD^{OE}$/$PFKFB3^{OE/GFP}$ cells were found more frequently at the tip position (N) than $NICD^{OE/GFP}$ cells (M). (O) The quantification of the fraction of tip cells with the indicated genotype is shown, revealing that PFKFB3 overexpression overcomes the disadvantage of $NICD^{OE/GFP}$ ECs to reach the tip (n = 30; *p < 0.05). Scale bars, 50 µm.

See also Figure S3.

levels improved tip cell formation, though only modestly (Figure S3C).

PFKFB3 Silencing Impairs Tip Cell Activity

To further document the importance of PFKFB3 during tip cell competition, we inhibited Notch signaling (which favors the tip cell phenotype) and examined whether PFKFB3 silencing affected their tip position. Spheroids of ECs in which Notch signaling was blocked by RNAi-mediated silencing ($NOTCH1^{KD/GFP}$) or DAPT treatment formed more numerous and longer sprouts (Figures 4H and 4I; Figures S3D and S3E), but PFKFB3 silencing in $NOTCH1^{KD/GFP}$ or DAPT-treated cells reduced the number and length of the vascular sprouts induced by Notch inhibition (Figures 4H and 4I; Figures S3D and S3E).

We also used mosaic spheroids containing a 1:1 mixture of WT^{RED} and $NOTCH1^{KD/GFP}$ cells. $NOTCH1^{KD/GFP}$ cells were more often detected at the tip (Figure 4J). However, when PFKFB3 was silenced in $NOTCH1^{KD/GFP}$ cells, the double-silenced cells were no longer preferentially present at the tip (Figure 4J). Thus, ECs lacking the genetic determinant of the stalk phenotype were less able to reside at the tip when their PFKFB3 levels were reduced. Similar results were obtained after treatment with MitoC, indicating that the observed findings were not only attributable to differences in proliferation (Figure S3F).

PFKFB3 Overexpression Improves Tip Cell Behavior

We further analyzed whether elevated PFKFB3 levels could overrule the stalk-cell-inducing activity of NICD. Vascular sprouting was impaired in spheroids of ECs overexpressing NICD ($NICD^{OE}$) (Figures 4K and 4L). Notably, however, overexpression of PFKFB3 in $NICD^{OE}$ cells overcame NICD's activity and restored vascular sprouting (Figures 4K and 4L), indicating that increased PFKFB3-driven glycolysis promoted sprouting, even when ECs were genetically instructed to adopt a stalk cell phenotype. Compared to tip cells, stalk cells have fewer and smaller filopodia and lamellipodia. Formation of lamellipodia was indeed impaired in $NICD^{OE}$ cells but was restored to near-normal levels in $NICD^{OE}/PFKFB3^{OE}$ cells (Figure S3G). We also used mosaic spheroids containing a 1:1 mixture of $mCherry^{+}$ (WT^{RED}) and GFP^{+} NICD-overexpressing ($NICD^{OE/GFP}$) ECs. Compared to WT^{red} cells, $NICD^{OE/GFP}$ cells were found less frequently at the tip (Figures 4M and 4O). However, $NICD^{OE/GFP}/PFKFB3^{OE/GFP}$ cells were present more frequently at the tip (Figures 4N and 4O). Mitotically inactivated ECs showed similar responses (Figure S3H).

PFKFB3 Promotes the Tip Cell Position In Vivo

We analyzed the hindbrain vasculature of E10.5 somite-matched chimeras generated by injecting $mCherryRed^{+}$ WT or $PFKFB3^{-/-}$ ES cells into CD-1 blastocysts. Hindbrains were stained for isolectin-B4 and the EC-specific transcription factor Erg to label ECs, and tip cells were identified as ECs with protrusions from where filopodia emerged. Compared to mosaic $mCherryRed^{+}$ WT ECs, 33% fewer $mCherryRed^{+}$ $PFKFB3^{-/-}$ ECs were present at the tip (Figures 5A–5E). We also used the zebrafish model to explore whether endothelial overexpression of PFKFB3 could overcome the stalk cell phenotype induced by overexpression of NICD. Using EC-selective *fli1*-promotor constructs, we generated transgenic *Fli1:EGFP*^{y1} zebrafish overexpressing mCherryRed and either NICD ($NICD^{OE/RED}$), PFKFB3 ($PFKFB3^{OE/RED}$), or both transgenes ($NICD^{OE}/PFKFB3^{OE/RED}$). All constructs expressed comparable transgene messenger RNA levels (data not shown), and the percentage of mosaic intersomitic vessels (ISVs) with an $mCherryRed^{+}$ cell at the tip was determined. Compared to 50% in control embryos, 60% of the mosaic ISVs contained an $mCherryRed^{+}$ tip cell in $PFKFB3^{OE/RED}$ embryos (Figures 5F–5M and 5V), showing that PFKFB3 overexpression provides a modest tip cell advantage in this assay. In $NICD^{OE/RED}$ embryos, only 22% of the ISVs contained an $mCherryRed^{+}$ tip cell while, notably, up to 67% of the ISVs contained an $mCherryRed^{+}$ tip cell in $NICD^{OE}/PFKFB3^{OE/RED}$ embryos (Figures 5N–5V). Thus, PFKFB3 was able to overcome NICD's pro-stalk activity.

Compartmentalization of PFKFB3

The aforementioned results show that PFKFB3 silencing affected EC motility, a process requiring remodeling of the cytoskeleton. Because respiration did not affect sprouting, we explored a possible link between glycolysis and the actin cytoskeleton. To analyze the cellular distribution of mitochondria in tip cells in vivo, we generated a transgenic $Mito^{EC}$: mouse expressing GFP in EC mitochondria. Isolectin-B4 staining of retinal ECs in vivo showed that mitochondria in tip cells were present in the perinuclear cytosol and in cytoplasmic protrusions at the base from where filopodia projected but were excluded from filopodia (Figures 6A–6C). Staining for the mitochondrial marker TOMM20 (Figure 6D) and time-lapse video imaging of $mCherry^{+}$ ECs in which mitochondria were labeled with Mito:EGFP (Movie S2) confirmed that mitochondria were excluded from lamellipodia.

We then analyzed the subcellular localization of glycolytic enzymes (including PFKFB3) by immunostaining. In spontaneously moving ECs, PFKFB3 was detectable in the cell body and lamellipodia (Figure 6E). Abundant PFKFB3 immunoreactivity was detected in the perinuclear cytosol. When analyzing PFKFB3 immunoreactive levels in a 300 nm single optical stack after pseudocolor conversion, PFKFB3-immunoreactive levels were comparable in lamellipodia and the cell body (Figure 6F). Quantification of PFKFB3 and F-actin immunoreactivity levels in single-stack images showed that PFKFB3 was enriched with F-actin in membrane ruffles at the leading front of lamellipodia, known to contain a meshwork of polymerized actin filaments (Figures 6G and 6H). Additional glycolytic enzymes, including the ATP-generating pyruvate kinase (PK) and phosphoglycerate kinase (PGK) and others, also colocalized with F-actin in lamellipodial ruffles (Figures S4A–S4H). Notably, unlike PKM2, PKM1, which is involved in ATP production rather than biosynthesis of macromolecules, also colocalized in lamellipodia (Figures S4I and S4J). Immunoprecipitation of PFKFB3 followed by immunoblotting for β-actin (Figure 6I) or mass spectrometry (Table S1) confirmed that PFKFB3 interacts with actin. Moreover, PFKFB3 was detectable in both the G- and F-actin cellular fractions (Figure 6J) but was more abundant in the F-actin fraction of motile than quiescent contact-inhibited ECs (Figure 6K). Notably, PFKFB3 was present in the perinuclear cytosol in

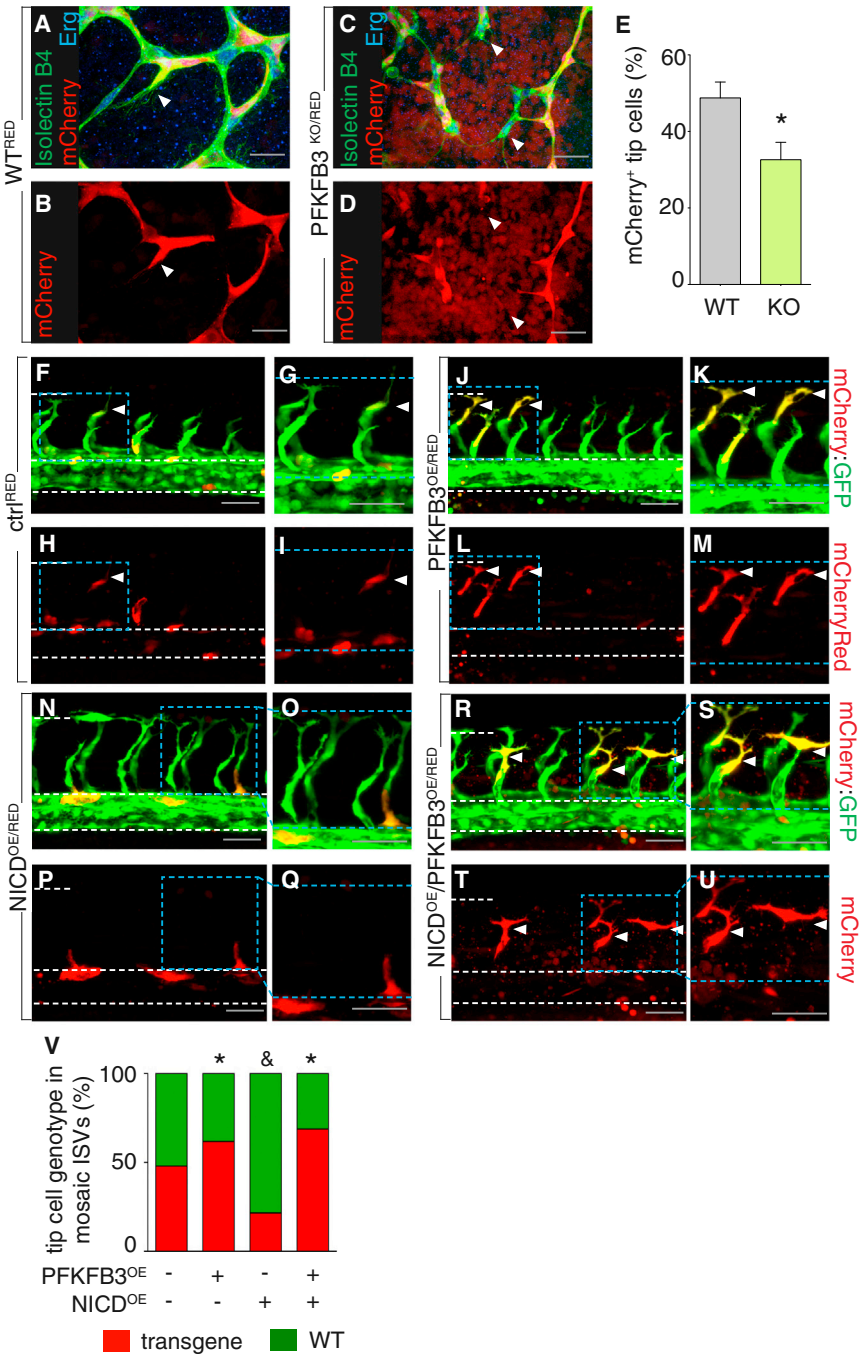

Figure 5. PFKFB3 Influences the Tip Position In Vivo

(A–E) Representative fluorescent image of the hindbrain vasculature in chimeric WT (A and B) and chimeric PFKFB3$^{-/-}$ (PFKFB3^{KO}) embryos (C and D) showing that mCherry^{+} WT^{RED} ECs contribute more frequently to the tip position than mCherry^{+} PFKFB3$^{KO/RED}$ ECs (arrowheads). Staining for Isolectin-B4 is shown in green, mCherry in red, and Erg in blue. (E) The quantification of the WT^{RED} and PFKFB3$^{KO/RED}$ tip cells is shown (mean ± SEM; n = 9–13; $p < 0.02$). Scale bars, 50 μm.

(F–V) Confocal images of GFP^{+} vessels in 24 hpf transgenic mosaic *fli1:EGFP*^{y1} embryos expressing only mCherryRed (ctrl^{RED}; F–I), coexpressing mCherry and PFKFB3 (PFKFB3$^{OE/RED}$; J–M), coexpressing mCherry and NICD (NICD$^{OE/RED}$; N–Q), or mCherry and NICD plus PFKFB3 (NICD^{OE}/PFKFB3$^{OE/RED}$; R–U) showing that overexpression of PFKFB3 promotes tip cell contribution and can overcome the NICD-induced tip cell disadvantage. (G, I, K, M, O, Q, S, U) Shown is a higher magnification of the boxes in (F), (H), (J), (L), (N), (P), (R), and (T). The arrowheads indicate mCherryRed^{+} ECs that reached the tip position. The dotted lines indicate the localization of the dorsal aorta and posterior cardinal vein (bottom) and the dorsal roof level (top). Scale bars, 50 μm. (V) The fraction of mosaic ISVs with the indicated tip cell genotype in *fli1:EGFP*^{y1} zebrafish embryos mosaically overexpressing NICD (NICD$^{OE/RED}$), PFKFB3 (PFKFB3$^{OE/RED}$), or both transgenes (NICD^{OE}/PFKFB3$^{OE/RED}$) is shown. Compared to controls, NICD$^{OE/RED}$ ECs were less frequently present at the tip, while PFKFB3$^{OE/RED}$ or NICD^{OE}/PFKFB3$^{OE/RED}$ ECs were present more frequently at the tip position, indicating that PFKFB3 overexpression overrules the NICD effect (n = 3–4 experiments with 55 ISVs/experiment; *$p < 0.05$ versus control; $^{\&}p < 0.05$ versus NICD$^{OE/RED}$).

contact-inhibited ECs but was relocated into the lamellipodia, protrusions, and cell-cell bridges in motile ECs (Figures S4K and S4L).

Furthermore, time-lapse video imaging after transfecting the ATP biosensor GO-ATeam in spontaneously motile ECs revealed high ATP levels in lamellipodia in leading membrane ruffles (Figure 6L; Movie S3). Compared to control cells, PFKFB3-silenced cells had 55% ± 5% fewer lamellipodial ATP hotspots, which were also 49% ± 9% smaller and contained 57% ± 2% lower levels of ATP (n = 4–5; $p < 0.001$) (Figure 6M). However, respiration blockers did not reduce lamellipodia ATP levels in the membrane ruffles (Figure 6N).

Cellular Adaptation to PFKFB3 Silencing

Finally, we explored whether the effects of PFKFB3 blockade were due to a general energy hypometabolism. However, PFKFB3 silencing did not alter the energy charge and ATP levels (Figures 7A and 7B), nor did it induce cell death as analyzed by measuring activated caspase 3 (Figures 7C and 7D) or LDH release (data not shown). PFKFB3-silenced cells showed no signs of endoplasmic reticulum, energy, or oxidative stress or of autophagy (Figures 7E–7H). PFKFB3 silencing did also not increase glucose oxidation and did not induce a switch to fatty acid oxidation or respiration (Figures 7I and 7J), which would be expected to occur when cells suffer severe energy deprivation from the blockage of glycolysis and need to compensate for such cellular energy

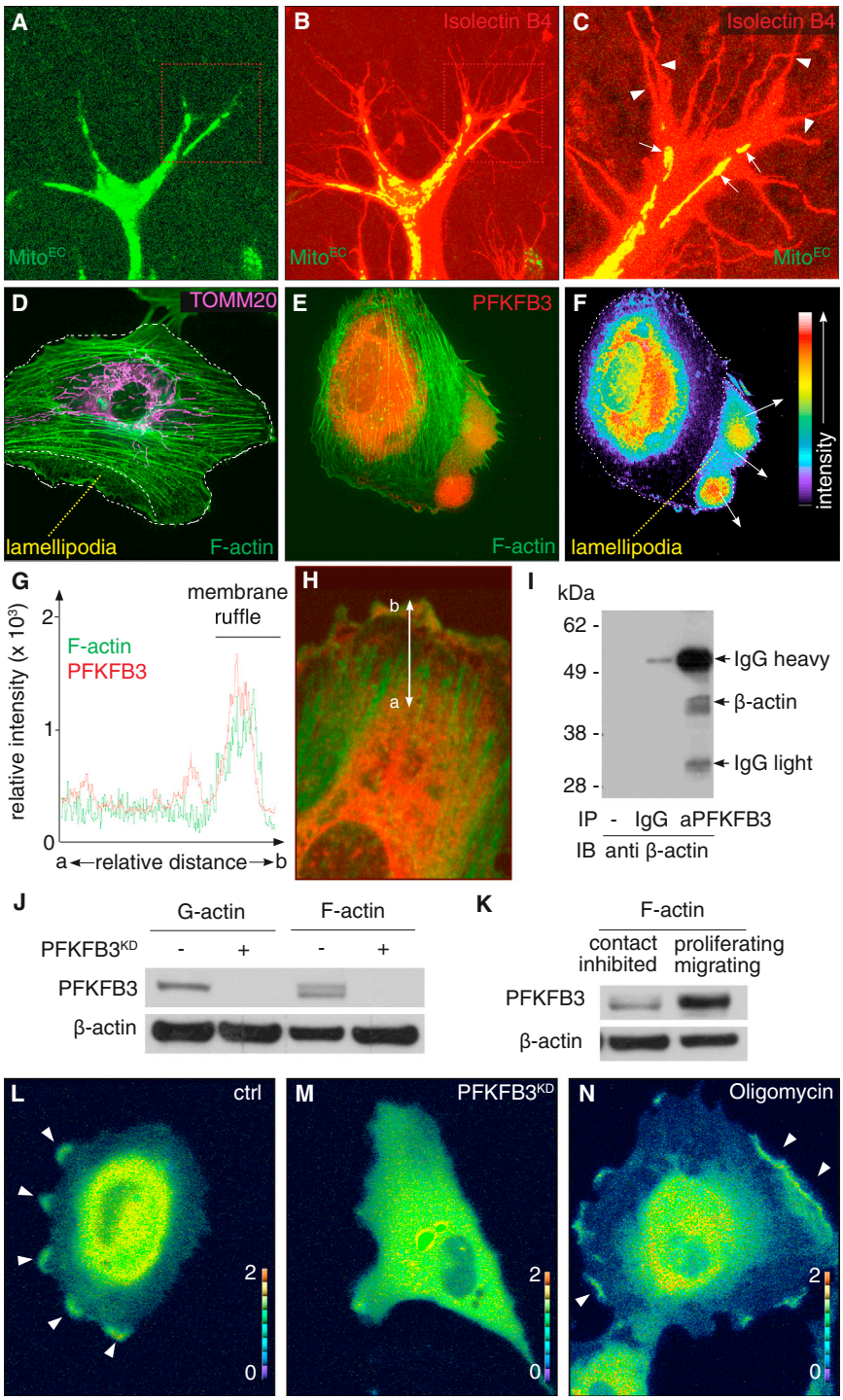

Figure 6. PFKFB3 Regulates the Actin-Remodeling Processes

(A–C) High-magnification images of tip cells in the retina of transgenic P4 Mito^{EC} reporter mice (A), stained for isolectin-B4 (B and C), revealing that mitochondria (green; arrows) are present in the cytosol and large cytosolic protrusions, but not inside filopodia (arrowheads). (C) Magnification of the boxed region in (A) and (B) (merger).

(D) High-magnification SIM images of ECs stained for the mitochondrial marker TOMM20 revealing that mitochondria are present in the central perinuclear cell body but excluded from the lamellipodia (denoted by a white dotted line).

(E and F) SIM imaging of sparsely seeded ECs immunostained for PFKFB3 revealing positive signal in the cell body and lamellipodia. (F) PFKFB3 pseudocolor conversion (from low [purple] to high [red]) in a 300 nm single optical stack is shown, revealing comparable levels in lamellipodia and the cell body. Arrows denote the migration direction.

(G and H) Quantification of the relative PFKFB3 and F-actin immunoreactive levels in single-stack images showing that PFKFB3 colocalized with F-actin in membrane ruffles. The line in (H) indicates the distance over which the immunoreactive levels were quantified (from point "a" to point "b").

(I) Immunoblotting (IB) for β-actin after immunoprecipitation (IP) of PFKFB3 from EC extracts using Dynabead-bound anti-PFKFB3 antibody (aPFKFB3), indicating that PFKFB3 interacts with actin (lane 3). Lane 1 and 2 show negative controls using naked beads and beads incubated with irrelevant B16F10.9 control antibody, respectively.

(J) Immunoblotting for PFKFB3 after ultracentrifugation-based separation of G-actin- and F-actin-enriched fractions showing that PFKFB3 is present in both fractions.

(K) Immunoblotting for PFKFB3 after ultracentrifugation-based separation of G-actin- and F-actin-enriched fractions showing that PFKFB3 is more abundantly associated with F-actin in proliferating/migrating than contact-inhibited cells.

(L–N) Snapshot pseudocolored images of time-lapse videos (Movie S3) of ECs expressing the ATP-biosensor GO-ATeam showing that membrane ruffles of lamellipodia (arrowheads) contain high ATP levels in control cells (L), but not in PFKFB3-silenced cells (PFKFB3^{KD}; M). Lamellipodial ATP levels remained unaffected by treatment with the mitochondrial respiration blocker oligomycin (N). Color bars indicate the orange fluorescent protein/GFP emission ratio (pseudocolor).

See also Figure S4, Movies S2 and S3, and Table S1.

stress. PFKFB3-silenced ECs were thus not in energy distress but rather adapted to a new metabolically balanced state. To maintain ATP levels, PFKFB3-silenced ECs decreased ATP consumption, as evidenced by a lower ADP/ATP ratio (Figure 7K) and reduced protein synthesis (Figure 7L) and EC proliferation (see above), all high-energy-demanding processes. Nonetheless, PFKFB3 silencing maintained extracellular matrix production (Figure 7M), promoted EC quiescence (Figure 7N), and increased the oxidative pentose phosphate pathway (oxPPP) (Figure 7O), thus showing that PFKFB3 knockdown did not cause general energy hypometabolism but rather suppressed the hypermetabolism induced by vessel sprouting. In conditions of stress, PFKFB3-silenced ECs even increased fatty acid oxidation (Figure 7P), likely to ensure redox homeostasis (Jeon et al., 2012).

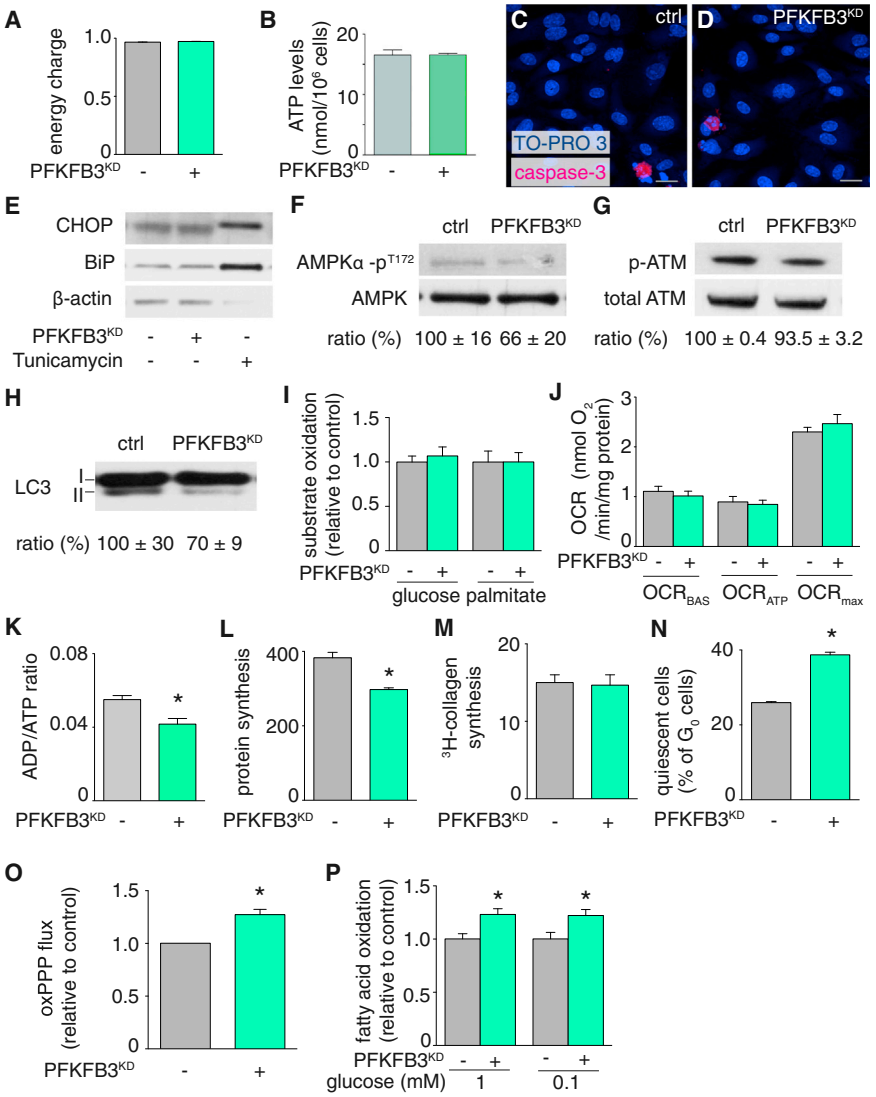

Figure 7. Adaptation to PFKFB3 Silencing

(A) PFKFB3 silencing did not affect the energy balance ([ATP] + 1/2 [ADP] / [ATP] + [ADP] + [AMP]) (mean ± SEM; n = 3; *p < 0.05).

(B) Quantification of ATP content showing that ATP levels were not affected in PFKFB3-silenced ($PFKFB3^{KD}$) cells (mean ± SEM, n = 6; p = nonsignificant [NS]).

(C and D) Caspase-3 immunostaining (red) in combination with TO-PRO3 nuclear staining (blue) showing that PFKFB3 silencing (D) did not cause apoptosis. Scale bar, 50 μm.

(E) Immunoblotting showing that PFKFB3 silencing did not alter expression levels of the ER stress markers BiP and CHOP. Tunicamycin treatment was used as positive control. Densitometric quantifications are shown below the lanes (mean ± SEM; n = 3; p = NS).

(F) Immunoblotting showing that PFKFB3 silencing did not alter the phospho-AMPK/AMPK ratio. Densitometric quantifications are shown below the lanes (mean ± SEM; n = 3; p = NS).

(G) Immunoblotting showing that PFKFB3 silencing did not alter the phospho-ATM/ATM ratio. Densitometric quantifications are shown below the lanes (mean ± SEM; n = 3; p = NS).

(H) Immunoblotting showing that PFKFB3 silencing did not induce autophagy, assessed via the LC3-II/LC3-I ratio. Densitometric quantifications are shown below the lanes (mean ± SEM; n = 3; p = NS).

(I) PFKFB3 silencing did not alter glucose oxidation or fatty acid oxidation (mean ± SEM; n = 3; p = NS).

(J) PFKFB3 silencing did not alter oxygen consumption rates (OCR) (mean ± SEM; n = 11; p = NS).

(K) PFKFB3 silencing reduced the ADP/ATP ratio (mean ± SEM; n = 3; *p < 0.05).

(L) Protein synthesis (HPG fluorescence intensity) was reduced in PFKFB3-silenced ECs (mean ± SEM; n = 3; *p < 0.05).

(M) ^{3}H-proline incorporation assay (10^3 dpm/hr/mg protein) showing that PFKFB3 silencing did not affect collagen synthesis (mean ± SEM; n = 3; p = NS).

(N) Fluorescence-activated cell sorting analysis of ECs, stained for Hoechst 33342 and EdU, showing a larger fraction of $Hoechst^{2N}Edu^{neg}$ cells in G_0 phase in PFKFB3-silenced cells (mean ± SEM, n = 5; *p < 0.001).

(O) PFKFB3 silencing increased the flux through the oxidative pentose phosphate pathway (oxPPP) (mean ± SEM; n = 3; p < 0.05).

(P) PFKFB3 silencing increased fatty acid oxidation under low-glucose (1 mM and 0.1 mM) conditions (mean ± SEM; n = 5; *p < 0.05).

DISCUSSION

Endothelial Cells Are Highly Glycolytic

ECs generated up to 85% of their ATP from glycolysis and were more glycolytic than other healthy cell types. In line with reports that ECs have a smaller mitochondrial volume fraction (5%) than oxidative hepatocytes (30%) and that mitochondria in ECs function as signaling hubs rather than metabolic powerhouses (Groschner et al., 2012), the flux through glucose, fatty acid, and glutamine oxidation in ECs was <1% of the glycolytic flux. The importance of glycolysis for ECs was illustrated by findings that PFKFB3 silencing reduced vessel sprouting, whereas inhibition or stimulation of respiration had no effect.

The dependence of ECs on glycolysis is at first sight surprising because quiescent ECs are in immediate contact with oxygen in the blood. Hence, ECs are exposed to sufficient oxygen for oxidative metabolism, yet they prefer aerobic glycolysis. This is likely due to various reasons. First, by consuming little oxygen, they can transfer more oxygen to perivascular cells. Second, when sprouting into avascular tissues, ECs become exposed to low levels of oxygen and glucose. Because glucose diffuses further away from vessels than oxygen (Buchwald, 2011; Gatenby and Gillies, 2004), ECs can still rely on anaerobic glycolysis to form vessels. Third, by maintaining a low oxidative metabolism, ECs minimize the production of reactive oxygen species, thereby providing protection against their high-oxygen milieu.

Fourth, glycolysis generates ATP more rapidly than oxidative metabolism, allowing ECs to meet the energy demands for dynamic rapid changes in motility. Finally, the glycolysis side pathways are necessary for the biosynthesis of macromolecules needed for cell mass duplication during cell division.

PFKFB3-Driven Glycolysis Regulates Sprouting

Silencing of PFKFB3 impaired vessel sprouting. These defects are due to effects on both migrating tip and proliferating stalk cells. In agreement with findings that cell proliferation requires glycolysis (Lunt and Vander Heiden, 2011), PFKFB3 inactivation reduced EC proliferation, implying that the impaired vessel formation was at least partially due to proliferation defects. However, PFKFB3 is also important for EC motility. First, the tip-cell-activating signal VEGF upregulated the levels of PFKFB3 and glycolysis, whereas the pro-stalk cell signal Notch had opposite effects. Second, PFKFB3 blockade suppressed whereas PFKFB3 overexpression stimulated the sprouting of mitotically inactivated ECs in spheroids. Furthermore, PFKFB3 silencing impaired the motility, lamellipodia/filopodia formation, and directional migration of EC monolayers, which could contribute to the impaired vessel outgrowth and branching in mice with endothelial PFKFB3 deficiency. Third, in mosaic competition assays in vitro (using mitotically inactivated cells) and in vivo, ECs with silenced PFKFB3 levels were underrepresented at the tip in baseline and in tip-cell-favoring conditions, whereas PFKFB3 overexpression promoted the ability of ECs to form tip cells in baseline conditions in some assays and promoted tip cell formation of cells overexpressing the pro-stalk cell signal NICD.

Notably, relative PFKFB3 levels did not alter the relative expression levels of tip or stalk cell genes, implying that a change in PFKFB3-driven glycolysis alone sufficed to promote tip cell activity. It is worth noting that no other signal has so far been reported to overcome NICD's potent pro-stalk cell activity, raising the question whether regulation of metabolism is a (perhaps even "the") key activity of Notch driving stalk cell formation. Given that tip and stalk cells dynamically interchange positions (Jakobsson et al., 2010), we speculate that an increased level of glycolysis does not permanently convert stalk cells into a fixed tip cell phenotype, but rather that varying levels of glycolysis dynamically codetermine the fluid tip versus stalk cell phenotype. These findings also raise other intriguing questions, such as for instance whether tip cells can only stay at the tip for as long as they have sufficient glycolysis. In any case, in parallel to control by genetic signals, PFKFB3-driven glycolysis also regulates vessel sprouting.

Compartmentalization of Glycolysis with Actin Cytoskeleton Remodeling

Filopodia and lamellipodia are essential for tip cells. Contraction and protrusion of these structures rely on actin cytoskeleton remodeling and require hydrolysis of large amounts of ATP. Mitochondria (0.5 to >4.0 μm) are too bulky to fit into thin filopodia and lamellipodia (250 nm wide and high, respectively) but are mostly present in the perinuclear cytosol, distant from the filopodial tip, which can be up to 10 μm long. Diffusion of ATP from distant mitochondria in the perinuclear cytosol may thus not be able to support the high and rapidly changing ATP demands for sustained motor activity at the tip.

Several lines of evidence suggest that glycolytic enzymes are compartmentalized with F-actin in lamellipodia during vascular sprouting. First, PFKFB3 and other glycolytic enzymes (including those generating ATP) were relocated from the perinuclear cytosol in contact-inhibited ECs into lamellipodia and cell protrusions and were enriched in leading membrane ruffles of motile cells. Interestingly, the pyruvate kinase isoenzyme involved in ATP production (PKM1) rather than macromolecular biosynthesis (PKM2) was present in lamellipodia. Second, ATP biosensor imaging revealed that lamellipodia contained "ATP hotspots," which were reduced when PFKFB3 was silenced, but not when respiration was blocked. Third, vessel branching was affected by inhibiting or stimulating glycolysis, but not by altering respiration. Fourth, PFKFB3 was associated with F-actin, and this fraction increased during EC migration.

The use of glycolysis to generate energy for motile structures may seem counterintuitive, as nearly 20-fold less ATP is produced per unit of glucose by glycolysis than by oxidative phosphorylation. Several reasons can explain this phenomenon. First, despite a low intrinsic yield, the yield of ATP generation by glycolysis can exceed that by glucose oxidation, as long as glucose is not limiting (DeBerardinis et al., 2008; Vander Heiden et al., 2009). Second, compartmentalization of glycolysis with F-actin offers advantages. By creating a "glycolytic hub," glycolytic enzymes are arranged on a cytomatrix in an assembly line, where metabolic substrates are passed from one enzyme to the next. Glycolytic enzymes are activated by actin and help in assembling actin microfilaments (Real-Hohn et al., 2010). The enzyme proximity and activation by actin favor maximal rates of reaction (al-Habori, 1995). Third, rapid extension/retraction of filopodia and lamellipodia may create an ATP drain for the cell body. Localizing the ATP supply to compartments where ATP is consumed can prevent catastrophic ATP depletion.

The link between glycolysis and actin is evolutionarily conserved, as glycolysis fuels other motile structures such as flagella of micro-organisms, tentacles of hydra, or cilia of eukaryotic cells (Baquer et al., 1975; Hereng et al., 2011; Pavlova, 2010). The relevance of this link is underscored by findings that expression of aldolase, incapacitated to bind actin, paralyzes fruit flies (Wojtas et al., 1997). PFKFB3 blockade might reduce angiogenesis also via other mechanisms. For instance, lactate stimulates angiogenesis via activation of HIF-1α and upregulation of *VEGFR2* (Hunt et al., 2007) or via inhibition of the oxygen sensor PHD2, activating a proangiogenic nuclear factor κB/interleukin-8 program (Végran et al., 2011). The reduced lactate levels upon PFKFB3 blockade could thus also suppress angiogenesis via these mechanisms. Also, PFKFB3 has been proposed to control cell proliferation via glycolysis-independent nuclear activities (Yalcin et al., 2009a). While perhaps relevant to explain the effects on EC proliferation, the effects of PFKFB3 on EC motility are more likely due to compartmentalization of glycolytic enzymes in the lamellipodia.

General Implications

To date, only genetic signals have been considered to control vessel sprouting. Our findings add an extra dimension to this

traditional concept and imply that metabolism also controls vessel sprouting. Aside from a genetic signature, tip and stalk cells thus likely also have a metabolic signature. While our study documented a role for glycolysis, other metabolic pathways might also influence vessel formation. In addition, it will be interesting to explore whether targeting PFKFB3 can reduce pathological angiogenesis.

EXPERIMENTAL PROCEDURES

More details can be found in the Extended Experimental Procedures.

Cell Culture and In Vitro Functional Assays

Freshly isolated primary HUVECs were used for metabolic evaluation, proliferation, migration, motility, and spheroid capillary sprouting assays and in cell-cycle assessments.

RNA and Protein Analysis

RNA expression analysis was done by quantitative RT-PCR. Immunoblotting of proteins and immunohistochemistry was performed using the antibodies listed in the Extended Experimental Procedures.

Metabolic Assays

Glycolysis and oxidation of other substrates were determined using radioactively labeled tracers.

Animal Models of Angiogenesis

Tg(fli1:EGFP)^{y1} zebrafish (Lawson and Weinstein, 2002) were subjected to Tol2-based transgenic overexpression. Quantification of sprouting of ISVs was done as explained in the Extended Experimental Procedures. Tamoxifen was injected intraperitoneally in mouse pups daily from postnatal day 1 to day 4. Eyes were fixed at postnatal day 5, and retinal flat mounts were prepared for vascular analysis as described (Phng et al., 2009). Embryonic hindbrain angiogenesis was assessed in E10.5–E11.5 embryos as described (Fantin et al., 2013). Experimental animal procedures were approved by the Institutional Animal Care and Research Advisory Committee of the University of Leuven.

Statistics

Data represent mean ± SEM of representative experiments unless otherwise stated. Unless otherwise indicated, statistical significance was calculated by standard t test (Prism v4.0b), and phenotype severity distributions were analyzed by the chi-square test. Estimated means, SEMs, and significance levels were calculated with the general linear model univariate statistical model (SPSS), considering experiment as covariate. $p < 0.05$ was considered as statistically significant.

ACCESSION NUMBERS

The microarray data have been deposited in the Gene Expression Omnibus (Edgar et al., 2002) under accession number GSE45750 (http://www.ncbi.nlm.nih.gov/geo/query/acc.cgi?acc=GSE45750).

SUPPLEMENTAL INFORMATION

Supplemental Information includes Extended Experimental Procedures, four figures, one table, and three movies and can be found with this article online at http://dx.doi.org/10.1016/j.cell.2013.06.037.

ACKNOWLEDGMENTS

We thank R. Adams for VE-cadherin(PAC)-Cre^{ERT2} mice and L. Notebaert for help with the figures. K.D.B., B.G., and I.S. are postdoctoral fellows of the FWO. M.G. and S.S. received funding as Emmanuel Vanderschueren fellows of the VLK. A.R.C. is funded by Fondazione Umberto Veronesi. B.W.W. received funding from the FWO and Marie Curie Foundation. A.K. and A.Q. are PhD FWO fellows. S.S. and B.C. are funded by the IWT. P.C. is supported by the Federal Government of Belgium (grant IUAP7/03), the Flemish Government (Methusalem funding), Concerted Research Activities Belgium (grant GOA2006/11), the FWO (grants G.0652.08, G.0692.09, G.0532.10, G.0817.11, and 1.5.202.10.N.00), the Foundation Leducq Transatlantic Network (ARTEMIS), and the ERC (advanced research grant EU-ERC269073). H.G. receives support from Cancer Research UK, the Lister Institute of Preventive Medicine, ARTEMIS, and the ERC (starting grant REshape 311719). L.K.P. and R.B. are supported by HFSP fellowships. P.C. is an inventor on patent applications claiming subject matter related to the results described in this paper. R.J.D. is a member of the scientific advisory board of Peleton Therapeutics. J.C. and S.T. are coinventors of U.S. patent 8,088,385 (PFKFB3 inhibitors for the treatment of proliferative cancer).

Received: March 5, 2012
Revised: April 2, 2013
Accepted: June 5, 2013
Published: August 1, 2013

REFERENCES

al-Habori, M. (1995). Microcompartmentation, metabolic channelling and carbohydrate metabolism. Int. J. Biochem. Cell Biol. *27*, 123–132.

Bando, H., Atsumi, T., Nishio, T., Niwa, H., Mishima, S., Shimizu, C., Yoshioka, N., Bucala, R., and Koike, T. (2005). Phosphorylation of the 6-phosphofructo-2-kinase/fructose 2,6-bisphosphatase/PFKFB3 family of glycolytic regulators in human cancer. Clin. Cancer Res. *11*, 5784–5792.

Baquer, N.Z., McLean, P., Hornbruch, A., and Wolpert, L. (1975). Positional information and pattern regulation in hydra: enzyme profiles. J. Embryol. Exp. Morphol. *33*, 853–867.

Benedito, R., Roca, C., Sörensen, I., Adams, S., Gossler, A., Fruttiger, M., and Adams, R.H. (2009). The notch ligands Dll4 and Jagged1 have opposing effects on angiogenesis. Cell *137*, 1124–1135.

Buchwald, P. (2011). A local glucose-and oxygen concentration-based insulin secretion model for pancreatic islets. Theor. Biol. Med. Model. *8*, 20.

Chesney, J., Mitchell, R., Benigni, F., Bacher, M., Spiegel, L., Al-Abed, Y., Han, J.H., Metz, C., and Bucala, R. (1999). An inducible gene product for 6-phosphofructo-2-kinase with an AU-rich instability element: role in tumor cell glycolysis and the Warburg effect. Proc. Natl. Acad. Sci. USA *96*, 3047–3052.

Claxton, S., Kostourou, V., Jadeja, S., Chambon, P., Hodivala-Dilke, K., and Fruttiger, M. (2008). Efficient, inducible Cre-recombinase activation in vascular endothelium. Genesis *46*, 74–80.

Clem, B., Telang, S., Clem, A., Yalcin, A., Meier, J., Simmons, A., Rasku, M.A., Arumugam, S., Dean, W.L., Eaton, J., et al. (2008). Small-molecule inhibition of 6-phosphofructo-2-kinase activity suppresses glycolytic flux and tumor growth. Mol. Cancer Ther. *7*, 110–120.

DeBerardinis, R.J., Lum, J.J., Hatzivassiliou, G., and Thompson, C.B. (2008). The biology of cancer: metabolic reprogramming fuels cell growth and proliferation. Cell Metab. *7*, 11–20.

Dobrina, A., and Rossi, F. (1983). Metabolic properties of freshly isolated bovine endothelial cells. Biochim. Biophys. Acta *762*, 295–301.

Edgar, R., Domrachev, M., and Lash, A.E. (2002). Gene Expression Omnibus: NCBI gene expression and hybridization array data repository. Nucleic Acid Res. *30*, 207–210.

Fantin, A., Vieira, J.M., Plein, A., Maden, C.H., and Ruhrberg, C. (2013). The embryonic mouse hindbrain as a qualitative and quantitative model for studying the molecular and cellular mechanisms of angiogenesis. Nat. Protoc. *8*, 418–429.

Gatenby, R.A., and Gillies, R.J. (2004). Why do cancers have high aerobic glycolysis? Nat. Rev. Cancer *4*, 891–899.

Geudens, I., and Gerhardt, H. (2011). Coordinating cell behaviour during blood vessel formation. Development *138*, 4569–4583.

Goidts, V., Bageritz, J., Puccio, L., Nakata, S., Zapatka, M., Barbus, S., Toedt, G., Campos, B., Korshunov, A., Momma, S., et al. (2012). RNAi screening in glioma stem-like cells identifies PFKFB4 as a key molecule important for cancer cell survival. Oncogene *31*, 3235–3243.

Graupera, M., Guillermet-Guibert, J., Foukas, L.C., Phng, L.K., Cain, R.J., Salpekar, A., Pearce, W., Meek, S., Millan, J., Cutillas, P.R., et al. (2008). Angiogenesis selectively requires the p110alpha isoform of PI3K to control endothelial cell migration. Nature *453*, 662–666.

Groschner, L.N., Waldeck-Weiermair, M., Malli, R., and Graier, W.F. (2012). Endothelial mitochondria—less respiration, more integration. Pflugers Arch. *464*, 63–76.

Harjes, U., Bensaad, K., and Harris, A.L. (2012). Endothelial cell metabolism and implications for cancer therapy. Br. J. Cancer *107*, 1207–1212.

Hereng, T.H., Elgstøen, K.B., Cederkvist, F.H., Eide, L., Jahnsen, T., Skålhegg, B.S., and Rosendal, K.R. (2011). Exogenous pyruvate accelerates glycolysis and promotes capacitation in human spermatozoa. Hum. Reprod. *26*, 3249–3263.

Hunt, T.K., Aslam, R.S., Beckert, S., Wagner, S., Ghani, Q.P., Hussain, M.Z., Roy, S., and Sen, C.K. (2007). Aerobically derived lactate stimulates revascularization and tissue repair via redox mechanisms. Antioxid. Redox Signal. *9*, 1115–1124.

Jakobsson, L., Franco, C.A., Bentley, K., Collins, R.T., Ponsioen, B., Aspalter, I.M., Rosewell, I., Busse, M., Thurston, G., Medvinsky, A., et al. (2010). Endothelial cells dynamically compete for the tip cell position during angiogenic sprouting. Nat. Cell Biol. *12*, 943–953.

Jeon, S.M., Chandel, N.S., and Hay, N. (2012). AMPK regulates NADPH homeostasis to promote tumour cell survival during energy stress. Nature *485*, 661–665.

Krützfeldt, A., Spahr, R., Mertens, S., Siegmund, B., and Piper, H.M. (1990). Metabolism of exogenous substrates by coronary endothelial cells in culture. J. Mol. Cell. Cardiol. *22*, 1393–1404.

Laing, R.A., Chiba, K., Tsubota, K., and Oak, S.S. (1992). Metabolic and morphologic changes in the corneal endothelium. The effects of potassium cyanide, iodoacetamide, and ouabain. Invest. Ophthalmol. Vis. Sci. *33*, 3315–3324.

Lawson, N.D., and Weinstein, B.M. (2002). In vivo imaging of embryonic vascular development using transgenic zebrafish. Dev. Biol. *248*, 307–318.

Leighton, B., Curi, R., Hussein, A., and Newsholme, E.A. (1987). Maximum activities of some key enzymes of glycolysis, glutaminolysis, Krebs cycle and fatty acid utilization in bovine pulmonary endothelial cells. FEBS Lett. *225*, 93–96.

Lunt, S.Y., and Vander Heiden, M.G. (2011). Aerobic glycolysis: meeting the metabolic requirements of cell proliferation. Annu. Rev. Cell Dev. Biol. *27*, 441–464.

Mertens, S., Noll, T., Spahr, R., Krützfeldt, A., and Piper, H.M. (1990). Energetic response of coronary endothelial cells to hypoxia. Am. J. Physiol. *258*, H689–H694.

Pavlova, G.A. (2010). Muscular waves contribute to gliding rate in the freshwater gastropod Lymnaea stagnalis. J. Comp. Physiol. A Neuroethol. Sens. Neural Behav. Physiol. *196*, 241–248.

Peters, K., Kamp, G., Berz, A., Unger, R.E., Barth, S., Salamon, A., Rychly, J., and Kirkpatrick, C.J. (2009). Changes in human endothelial cell energy metabolic capacities during in vitro cultivation. The role of "aerobic glycolysis" and proliferation. Cell. Physiol. Biochem. *24*, 483–492.

Phng, L.K., Potente, M., Leslie, J.D., Babbage, J., Nyqvist, D., Lobov, I., Ondr, J.K., Rao, S., Lang, R.A., Thurston, G., and Gerhardt, H. (2009). Nrarp coordinates endothelial Notch and Wnt signaling to control vessel density in angiogenesis. Dev. Cell *16*, 70–82.

Potente, M., Gerhardt, H., and Carmeliet, P. (2011). Basic and therapeutic aspects of angiogenesis. Cell *146*, 873–887.

Real-Hohn, A., Zancan, P., Da Silva, D., Martins, E.R., Salgado, L.T., Mermelstein, C.S., Gomes, A.M., and Sola-Penna, M. (2010). Filamentous actin and its associated binding proteins are the stimulatory site for 6-phosphofructo-1-kinase association within the membrane of human erythrocytes. Biochimie *92*, 538–544.

Ros, S., Santos, C.R., Moco, S., Baenke, F., Kelly, G., Howell, M., Zamboni, N., and Schulze, A. (2012). Functional metabolic screen identifies 6-phosphofructo-2-kinase/fructose-2,6-biphosphatase 4 as an important regulator of prostate cancer cell survival. Cancer Discov. *2*, 328–343.

Spolarics, Z., Lang, C.H., Bagby, G.J., and Spitzer, J.J. (1991). Glutamine and fatty acid oxidation are the main sources of energy for Kupffer and endothelial cells. Am. J. Physiol. *261*, G185–G190.

Van Schaftingen, E., Lederer, B., Bartrons, R., and Hers, H.G. (1982). A kinetic study of pyrophosphate: fructose-6-phosphate phosphotransferase from potato tubers. Application to a microassay of fructose 2,6-bisphosphate. Eur. J. Biochem. *129*, 191–195.

Vander Heiden, M.G., Cantley, L.C., and Thompson, C.B. (2009). Understanding the Warburg effect: the metabolic requirements of cell proliferation. Science *324*, 1029–1033.

Végran, F., Boidot, R., Michiels, C., Sonveaux, P., and Feron, O. (2011). Lactate influx through the endothelial cell monocarboxylate transporter MCT1 supports an NF-κB/IL-8 pathway that drives tumor angiogenesis. Cancer Res. *71*, 2550–2560.

Wojtas, K., Slepecky, N., von Kalm, L., and Sullivan, D. (1997). Flight muscle function in Drosophila requires colocalization of glycolytic enzymes. Mol. Biol. Cell *8*, 1665–1675.

Yalcin, A., Clem, B.F., Simmons, A., Lane, A., Nelson, K., Clem, A.L., Brock, E., Siow, D., Wattenberg, B., Telang, S., and Chesney, J. (2009a). Nuclear targeting of 6-phosphofructo-2-kinase (PFKFB3) increases proliferation via cyclin-dependent kinases. J. Biol. Chem. *284*, 24223–24232.

Yalcin, A., Telang, S., Clem, B., and Chesney, J. (2009b). Regulation of glucose metabolism by 6-phosphofructo-2-kinase/fructose-2,6-bisphosphatases in cancer. Exp. Mol. Pathol. *86*, 174–179.